arXiv:1207.5327v2 [hep-ph] 25 Jul 2012

Thermal Bottomonium Suppression

Michael Strickland

Physics Department, Gettysburg College, Gettysburg, PA 17325 United States

Abstract. I discuss recent calculations of the thermal suppression of bottomonium states in relativistic heavy ion collisions. I present results for the inclusive $\Upsilon(1s)$ and $\Upsilon(2s)$ suppression as a function of centrality. I compare with recent CMS preliminary data available at central rapidities and make predictions at forward rapidities which are within the acceptance of the ALICE dimuon spectrometer.

Keywords: Quarkonium Suppression, Relativistic Heavy Ion Collision, Quark-Gluon Plasma
PACS: 11.15Bt, 04.25.Nx, 11.10Wx, 12.38Mh

INTRODUCTION

The purpose of ongoing and upcoming heavy ion collision experiments at the Relativistic Heavy Ion Collider (RHIC) and the Large Hadron Collider (LHC) is to study the behavior of nuclear matter at high energy density, $\varepsilon \gg 1\ \text{GeV}/\text{fm}^3$. At such high energy densities one expects to create a deconfined quark gluon plasma (QGP). One of the key observables measured in the experiments is the relative yield of heavy quarkonium production relative to that in proton-proton collisions scaled by the number of nucleon collisions, R_{AA}. Early studies predicted that at high temperatures Debye screening would lead to the dissolution of hadronic bound states [1]. Therefore, one might be able to use the relative suppression of heavy quark bound states as a "smoking gun" for the creation of the quark gluon plasma. Over the last 25 years most of the interest has been focused on the suppression of heavy quark-antiquark bound states following early predictions of thermal J/Ψ suppression [2, 3]. In recent years interest has shifted to bound states of bottom and anti-bottom quarks (bottomonium) for the following reasons

- Bottom quarks ($m_b \simeq 4.2$ GeV) are more massive than charm quarks ($m_c \simeq 1.3$ GeV) and as a result the heavy quark effective theories underpinning phenomenological applications are on much surer footing.
- The masses of bottomonium states ($m_\Upsilon \approx 10$ GeV) are much higher than the temperatures ($T \lesssim 1$ GeV) generated in relativistic heavy ion collisions. As a result, bottomonium production will be dominated by initial hard scatterings.
- Since bottom quarks and anti-quarks are relatively rare within the plasma, the probability for regeneration of bottomonium states through recombination is much smaller than for charm quarks.
- Due to their higher mass, the effects of initial state nuclear suppression are expected to be reduced.

As a result one expects the bottomonium system to be a cleaner probe of the quark gluon plasma than the charmonium system for which the modeling has necessarily become quite involved. For this reason I will focus on the bottomonium states in this paper and only consider the thermal suppression of these states, ignoring initial state effects and any possible thermal generation or recombination.

In this paper I will review recent theoretical calculations of bottomonium suppression at energies probed in relativistic heavy ion collisions at the Large Hadron Collider (LHC). I will present a brief overview of the important aspects of the calculation and refer the reader to Refs. [4, 5] for details. I will compare my prediction for inclusive $\Upsilon(1s)$ and $\Upsilon(2s)$ suppression with recent preliminary data to be released from the CMS collaboration. In addition, I present new predictions for $\Upsilon(1s)$ and $\Upsilon(2s)$ suppression at forward rapidities in order facilitate comparison with results forthcoming from the ALICE collaboration.

THEORETICAL METHODS

In recent years there have been important theoretical developments in heavy quarkonium theory. Chief among these are the first-principles calculations of imaginary-valued contributions to the heavy quark potential. The first calculation of the leading-order perturbative imaginary part of the potential due to gluonic Landau damping was performed by Laine et al. [6]. Since then an additional imaginary-valued contribution to the potential coming from singlet to octet transitions has also been computed using the effective field theory approach [7]. These imaginary-valued contributions to the potential are related to quarkonium decay processes in the plasma. The consequences of such imaginary parts on heavy quarkonium spectral functions [8, 9], perturbative thermal widths [6, 10], in a T-matrix approach [11–13], and in stochastic real-time dynamics [14] have recently been studied.

In addition, there have been significant advances in the dynamical models used to simulate plasma evolution. In particular, there has been a concerted effort to understand the effects of plasma momentum-space anisotropies generated by the rapid longitudinal expansion of the matter along the beamline direction. Dynamical models are now able to describe the anisotropic hydrodynamical evolution in full (3+1)-dimensional simulations [15–20]. This is important because momentum-space anisotropies can have a significant impact on quarkonium suppression since in regions of high momentum-space anisotropy one expects reduced quarkonium binding [21–25]. In Refs. [4, 5] the dynamical evolution of the anisotropic plasma was combined with the real and imaginary parts of the binding energy obtained using modern complex-valued potentials.

Potential model and binding energies

The heavy quark potential has real and imaginary parts, $V = \Re[V] + i\Im[V]$. Here I will focus on a model in which the real part of the potential is obtained from internal energy of the system since models based on the free energy seem to be incapable of reproducing either the LHC or RHIC $R_{AA}[\Upsilon]$. The real part of the potential is given by [5]

$$\Re[V] = -\frac{a}{r}(1+\mu\, r)\, e^{-\mu\, r} + \frac{2\sigma}{\mu}\left[1 - e^{-\mu\, r}\right] - \sigma\, r\, e^{-\mu\, r} - \frac{0.8\,\sigma}{m_Q^2 r}\,, \tag{1}$$

where $a = 0.385$ and $\sigma = 0.223$ GeV^2 [26] and the last term is a temperature- and spin-independent finite quark mass correction taken from Ref. [27]. In this expression $\mu = \mathscr{G}(\xi,\theta)m_D$ is an anisotropic Debye mass where $\mathscr{G}$ is a rather complicated function which depends on the degree of plasma momentum-space anisotropy, ξ, and the angle of the line connecting the quark-antiquark pair with respect to the beamline direction, θ, and m_D is the isotropic Debye mass [5]. In the limit $\xi \to 0$ one has $\mathscr{G} = 1$.

The imaginary part of the potential $\Im[V]$ is obtained from a leading order perturbative calculation which was performed in the small anisotropy limit

$$\Im[V] = -\alpha_s C_F T \left\{ \phi(r/m_D) - \xi \left[\psi_1(r/m_D,\theta) + \psi_2(r/m_D,\theta) \right] \right\}, \tag{2}$$

where ϕ, ψ_1, and ψ_2 can be expressed in terms of hypergeometric functions [24].

After combining the real and imaginary parts of the potential, the 3d Schrödinger equation is solved numerically to obtain the real and imaginary parts of the binding energy as a function of ξ and $p_{\rm hard}$ [25, 28]. The imaginary part of the binding energy is related to the width of the state

$$\Gamma(\tau,\mathbf{x}_\perp,\varsigma) = \begin{cases} 2\Im[E_{\rm bind}(\tau,\mathbf{x}_\perp,\varsigma)] & \Re[E_{\rm bind}(\tau,\mathbf{x}_\perp,\varsigma)] > 0 \\ 10\ \text{GeV} & \Re[E_{\rm bind}(\tau,\mathbf{x}_\perp,\varsigma)] \le 0 \end{cases} \tag{3}$$

where $\varsigma = \text{arctanh}(z/t)$ is the spatial rapidity. The value of 10 GeV in the second case is chosen to be large in order to quickly suppress states which are fully unbound (which is the case when the real part of the binding energy is negative).

Dynamical Model

The dynamical model used gives the spatio-temporal evolution of the typical transverse momentum of the plasma partons, $p_{\rm hard}(\tau,\mathbf{x})$, and the plasma momentum-space anisotropy, $\xi(\tau,\mathbf{x})$, both of which are specified in the local rest frame of the plasma. The widths obtained from solution of the 3d Schrödinger equation are then integrated and exponentiated to compute the relative number of states remaining at a given proper time. This quantity is then averaged over the transverse plane taking into account the local conditions in the plasma and weighting by the spatial probability distribution for bottomonium production which is given by the number of binary collisions computed in the Glauber model with a Woods-Saxon distribution for each nucleus. For the temporal integration the initial time is set by the formation time of the state in question.

The resulting R_{AA} is a function of the transverse momentum, p_T, the rapidity ς, and the nuclear impact parameter b. To compare to experimental results transverse momentum cuts are applied using a $n(p_T) = n_0 E_T^{-4}$ spectrum. In addition, any cuts on the rapidity due to detector acceptance and centrality are applied as needed. For details of the dynamical model and R_{AA} computation I refer the reader to Ref. [5].

Initial conditions

For the initial conditions I use a Woods-Saxon distribution for each nucleus and determine the transverse dependence of the initial temperature via the third root of the number of participants (wounded nucleons). In the spatial rapidity direction I will

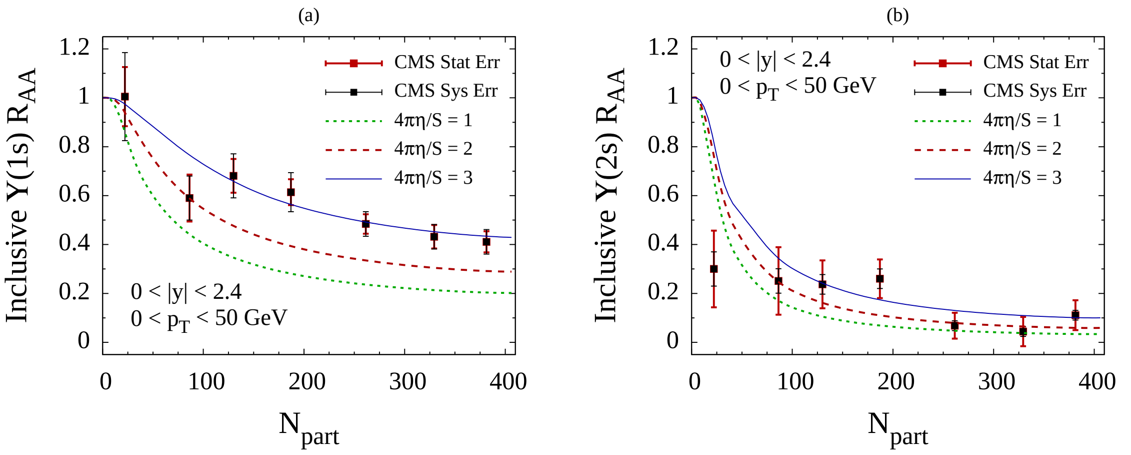

FIGURE 1. Predictions for the central rapidity inclusive (a) $\Upsilon(1s)$ and (b) $\Upsilon(2s)$ suppression including feed-down as a function of $N_{\rm part}$ along with recent preliminary data from the CMS collaboration. Three curves show the variation with the assumed shear viscosity to entropy ratio.

investigate two possible temperature profiles: (a) a broad plateau containing a boost-invariant central region with Gaussian limited-fragmentation at large rapidity

$$n(\varsigma) = n_0 \exp(-(|\varsigma| - \varsigma_{\rm flat}/2)^2/2\sigma_\varsigma^2)\, \Theta(|\varsigma| - \varsigma_{\rm flat}/2)\,, \tag{4}$$

where $\varsigma_{\rm flat} = 10$ is the width of the central rapidity plateau, $\sigma_\varsigma = 0.5$ is the width of the limited fragmentation tails, and n_0 is the number density at central rapidity [29]; and (b) a Gaussian motivated by low-energy fits to pion spectra

$$n(\varsigma) = n_0 \exp(-\varsigma^2/2\sigma_\varsigma^2) \quad \text{with} \quad \sigma_\varsigma^2 = 0.64 \cdot 8\, c_s^2 \ln\left(\sqrt{s_{NN}}/2m_p\right)/3(1-c_s^4)\,, \tag{5}$$

where $c_s = 1/\sqrt{3}$ is the sound velocity, $m_p = 0.938$ GeV is the proton mass, and $\sqrt{s_{NN}}$ is the nucleon-nucleon center-of-mass energy [5, 30]. The temperature distribution is given by $T \sim n^{1/3}$. I note that (4) has the advantage that it has been tuned to successfully describe the rapidity dependence of the elliptic flow in LHC heavy ion collisions.

RESULTS AND CONCLUSIONS

When considering the suppression of the $\Upsilon(1s)$ and $\Upsilon(2s)$ states it is important to include the effect of feed-down from higher excited states. In pp collisions only approximately 51% of $\Upsilon(1s)$ states come from direct production and similarly for the $\Upsilon(2s)$. One can compute the inclusive suppression of a state using $R_{AA}^{\rm full}[\Upsilon(ns)] = \sum_{i \in {\rm states}} f_i R_{i,AA}$ where f_i are the feed-down fractions and $R_{i,AA}$ is the direct suppression of each state which decays into the $\Upsilon(ns)$ state being considered. Here I will use $f_i = \{0.510, 0.107, 0.008, 0.27, 0.105\}$ for the $\Upsilon(1s)$, $\Upsilon(2s)$, $\Upsilon(3s)$, χ_{b1}, and χ_{b2} feed-down to $\Upsilon(1s)$, respectively [31]. For the inclusive $\Upsilon(2s)$ production I use $f_i = \{0.500, 0.500\}$ for the $\Upsilon(2s)$ and $\Upsilon(3s)$ states, respectively. For details of the computation of the direct R_{AA} for each state see Ref. [5].

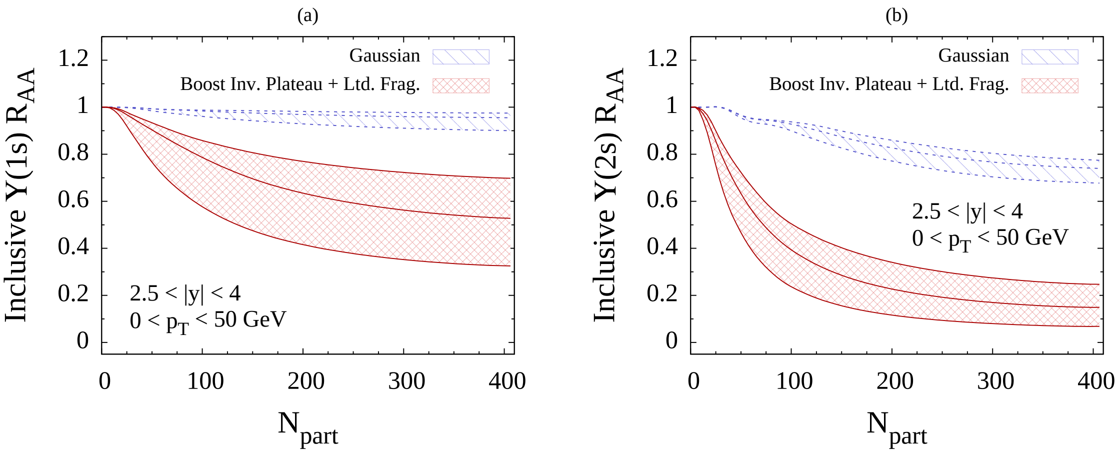

FIGURE 2. Predictions for the inclusive (a) $\Upsilon(1s)$ and (b) $\Upsilon(2s)$ including feed-down as a function of $N_{\rm part}$ at forward rapidities $2.5 \leq y \leq 4.0$. Bands show variation with η/S with the bottom, middle, and top lines in each set corresponding to $4\pi\eta/S = \{1,2,3\}$, respectively.

In Fig. 1 I compare to preliminary data on the inclusive $\Upsilon(1s)$ and $\Upsilon(2s)$ suppression available from the CMS collaboration [32]. For this figure I used a broad rapidity plateau as the initial density profile as specified in Eq. (4). The central temperatures were taken to be $T_0 = \{520, 504, 494\}$ MeV at $\tau_0 = 0.3$ fm/c for $4\pi\eta/S = \{1,2,3\}$, respectively, in order to fix the final charged multiplicity to $dN_{\rm ch}/dy \simeq 1400$ in each case. As can been seen from this figure, the predictions agree reasonably well with the available data. The data seem to prefer the largest value of η/S shown; however, there is a $\pm 14\%$, $\pm 21\%$ 1s, 2s global uncertainty reported by CMS, making it hard to draw firm conclusions.

Next I consider forward rapidities. The ALICE forward muon spectrometer detects charmonium and bottomonium states via dimuon decay with an acceptance that covers the pseudorapidity interval $2.5 \leq y \leq 4.0$ with a resolution of approximately 100 MeV. For more information on ALICE's dimuon capabilities see e.g. [33–36] and references therein. One of the key questions that such forward rapidity measurements will be able to answer is the nature of the temperature distribution of the plasma at forward rapidities.

In order to illustrate this in Fig. 2 I show predictions for the inclusive suppression of $\Upsilon(1s)$ and $\Upsilon(2s)$ states using either Eq. (4) or Eq. (5) as the initial rapidity profile of the density. As can be seen from this figure there is a rather large effect. The boost-invariant plateau with limited fragmentation (4) is the one which is canonically used in heavy-ion models and follows naturally from the Bjorken picture, while the Gaussian assumption (5) is more in line with the Landau picture. I would expect, based on ability of the Bjorken-like picture to describe the rapidity dependence of elliptic flow [29], that this is, in fact, what one would see in the experiment; however, for completeness sake I show the Gaussian in order to demonstrate that the future ALICE results in this region of phase space could easily discern between the two possibilities.

To conclude, in this paper I have attempted to review recent calculations of bottomonium suppression in LHC heavy ion collisions. I presented comparisons of prior predictions with CMS preliminary data for inclusive $\Upsilon(1s)$ and $\Upsilon(2s)$ suppression. In addition, I have made new predictions for inclusive $\Upsilon(1s)$ and $\Upsilon(2s)$ at forward rapidities within the ALICE acceptance. I found that one can easily distinguish between the so-called Landau and Bjorken pictures of heavy ion collisions with such forward rapidity data.

ACKNOWLEDGMENTS

I thank Guillermo Breto Rangel discussions concerning the CMS preliminary results on $\Upsilon(1s)$ and $\Upsilon(2s)$ suppression. I thank Debasish Das for discussions about ALICE's forward rapidity capabilities. This work was supported by NSF grant No. PHY-1068765 and the Helmholtz International Center for FAIR LOEWE program.

REFERENCES

1. E. V. Shuryak, *Phys. Rept.* **61**, 71–158 (1980).
2. T. Matsui, and H. Satz, *Phys. Lett.* **B178**, 416 (1986).
3. F. Karsch, M. T. Mehr, and H. Satz, *Z. Phys.* **C37**, 617 (1988).
4. M. Strickland, *Phys.Rev.Lett.* **107**, 132301 (2011), `1106.2571`.
5. M. Strickland, and D. Bazow, *Nucl.Phys.* **A879**, 25–58 (2012), `1112.2761`.
6. M. Laine, O. Philipsen, P. Romatschke, and M. Tassler, *JHEP* **03**, 054 (2007), `hep-ph/0611300`.
7. N. Brambilla, J. Ghiglieri, A. Vairo, and P. Petreczky, *Phys. Rev.* **D78**, 014017 (2008), `0804.0993`.
8. Y. Burnier, M. Laine, and M. Vepsalainen, *JHEP* **0801**, 043 (2008), `0711.1743`.
9. C. Miao, A. Mocsy, and P. Petreczky, *Nucl. Phys.* **A855**, 125–132 (2011), `1012.4433`.
10. N. Brambilla, M. A. Escobedo, J. Ghiglieri, J. Soto, and A. Vairo, *JHEP* **09**, 038 (2010), `1007.4156`.
11. L. Grandchamp, S. Lumpkins, D. Sun, H. van Hees, and R. Rapp, *Phys.Rev.* **C73**, 064906 (2006), `hep-ph/0507314`.
12. R. Rapp, D. Blaschke, and P. Crochet (2008), `0807.2470`.
13. F. Riek, and R. Rapp, *New J. Phys.* **13**, 045007 (2011), `1012.0019`.
14. Y. Akamatsu, and A. Rothkopf (2011), `1110.1203`.
15. W. Florkowski, and R. Ryblewski, *Phys.Rev.* **C83**, 034907 (2011), `1007.0130`.
16. M. Martinez, and M. Strickland, *Nucl. Phys.* **A848**, 183–197 (2010), `1007.0889`.
17. R. Ryblewski, and W. Florkowski, *J.Phys.G* **G38**, 015104 (2011), `1007.4662`.
18. M. Martinez, and M. Strickland, *Nucl.Phys.* **A856**, 68–87 (2011), `1011.3056`.
19. M. Martinez, R. Ryblewski, and M. Strickland, *Phys.Rev.* **C85**, 064913 (2012), `1204.1473`.
20. R. Ryblewski, and W. Florkowski, *Phys.Rev.* **C85**, 064901 (2012), `1204.2624`.
21. A. Dumitru, Y. Guo, and M. Strickland, *Phys. Lett.* **B662**, 37–42 (2008), `0711.4722`.
22. A. Dumitru, Y. Guo, A. Mocsy, and M. Strickland, *Phys.Rev.* **D79**, 054019 (2009), `0901.1998`.
23. Y. Burnier, M. Laine, and M. Vepsalainen, *Phys.Lett.* **B678**, 86–89 (2009), `0903.3467`.
24. A. Dumitru, Y. Guo, and M. Strickland, *Phys.Rev.* **D79**, 114003 (2009), `0903.4703`.
25. M. Margotta, K. McCarty, C. McGahan, M. Strickland, and D. Yager-Elorriaga, *Phys.Rev.* **D83**, 105019 (2011), `1101.4651`.
26. P. Petreczky, *J.Phys.G* **G37**, 094009 (2010), `1001.5284`.
27. G. S. Bali, K. Schilling, and A. Wachter, *Phys. Rev.* **D56**, 2566–2589 (1997), `hep-lat/9703019`.
28. M. Strickland, and D. Yager-Elorriaga, *J. Comput. Phys.* **229**, 6015–6026 (2010), `0904.0939`.
29. B. Schenke, S. Jeon, and C. Gale (2011), `1102.0575`.
30. M. Bleicher (2005), `hep-ph/0509314`.
31. A. A. Affolder, et al., *Phys.Rev.Lett.* **84**, 2094–2099 (2000), `hep-ex/9910025`.
32. CMS Collaboration, Observation of $\Upsilon(nS)$ suppression (2012), URL `https://twiki.cern.ch/twiki/bin/view/CMSPublic/PhysicsResultsHIN11011`.
33. C. Fabjan, and J. Schukraft (2011), `1101.1257`.
34. D. Das (2011), `1111.5946`.
35. D. Das, *Nucl.Phys.* **A862-863**, 223–230 (2011), `1102.2071`.
36. L. S. Kisslinger, and D. Das (2012), `1207.3296`.